



Artificial neural network modeling of Cr(VI) photocatalytic reduction with TiO₂-P25 nanoparticles using the results obtained from response surface methodology optimization

Maryam Sabonian, Mohammad A. Behnajady*

Department of Chemistry, College of Science, Tabriz Branch, Islamic Azad University, Tabriz, Iran, Tel. +98 41 33396136; Fax: +98 41 33333458; emails: behnajady@gmail.com, behnajady@iaut.ac.ir (M.A. Behnajady)

Received 13 April 2014; Accepted 2 September 2014

ABSTRACT

In this study, the nanoparticles of TiO₂-P25 in the slurry situation were used for photoreduction of Cr(VI). The experiments were conducted in different operational conditions such as initial concentration of Cr(VI), varying dosages of photocatalyst, and different irradiation times and pHs. Using the response surface methodology, the mathematical equation for estimating the percentage of Cr(VI) photocatalytic removal was obtained. For the first time, the results from this model were utilized for modeling the process by artificial neural networks (ANN). The comparison of the analyzed data obtained from ANN and the experimental data showed that the method was highly efficient in the modeling of process. The relative importance of the parameters affecting the process evaluated by the weights from ANN indicated that pH was the most important factor in photocatalytic reduction of Cr(VI).

Keywords: Heterogeneous photocatalysis; Photocatalytic reduction; Cr(VI); Titanium dioxide nanoparticles; Artificial neural networks; Response surface methodology

1. Introduction

Cr(VI) is a toxic pollutant found in industrial wastewaters [1–4]. Chromium exists in two oxidation forms of Cr(III) and Cr(VI) [5–7]. Cr(III) is much less toxic and mobile than Cr(VI). In fact, Cr(III) in low doses is an essential dietary mineral [8,9]. Compared with other heavy metals, chromium has a wider range of applications. It is used in tanning leather and manufacturing paint, pigments [10–13], photographic materials, steel alloys [14], glass, ceramics, and fungicides [15]. It is also used in cement industries, mining, water coolant of nuclear power plants, and petroleum refining processes [10,14]. The concentration of Cr(VI)

in industrial wastewater ranges between 0.5 and 270 mg L⁻¹ [16]. The hexavalent state may be found in the form of chromic acid (H₂CrO₄), dichromate anion (Cr₂O₇²⁻), hydrogen chromate anion (HCrO₄⁻), or chromate anion (CrO₄²⁻) [1]. The hexavalent form is 500 times more toxic than the trivalent form [17]. The toxic effects of Cr(VI) include skin irritation, lung cancer, and harmful effects on kidney, liver, and gastric [18,19]. Common methods of Cr(VI) removal include chemical reduction, ion exchange, adsorption on coal or active carbon, and bacterial reduction [20,21]. The photocatalytic reduction of Cr(VI) is possible with semiconductors such as ZnO, TiO₂, ZnS, CdS, and WO₃ [22,23]. Since late twentieth century, TiO₂ has been used as an efficient photocatalyst, because of its

*Corresponding author.

high photocatalytic activity, nontoxic nature, good stability, and low-cost fabrication [8,14].

Response surface methodology (RSM), which began with the works of Box and Wilson in 1951, refers to a set of statistical and mathematical techniques that contribute to the processes of development, improvement, and optimization and can simultaneously determine the optimum of several variables with the minimum number of experiments and quantitative data and by offering appropriate experimental design [24,25]. Using RSM, it is possible to estimate linear, interaction, and quadratic effects of the factors, and to develop a prediction model for the response. [26–29]. The first- and second-order models are in the form of Eqs. (1) and (2), respectively:

$$y = \beta_0 + \sum_{i=1}^k \beta_i x_i + \varepsilon \quad (1)$$

$$y = \beta_0 + \sum_{i=1}^k \beta_i x_i + \sum_{i=1}^k \beta_{ii} x_i^2 + \sum_i \sum_j \beta_{ij} x_i x_j + \varepsilon \quad (2)$$

where y is the response, β_0 is the constant coefficient, β_i is the coefficient of linear effects, β_{ii} is the coefficient of squared effects, β_{ij} is the coefficient of interaction effects, x_i and x_j are the variables, and ε is the random error [30–32]. To distinguish the levels from each other, codes such as (+1), (0), and (–1) are used. This simplifies recording the experimental conditions and laboratory processes. Factorial levels are selected in a way that the highest level is (+ α), the lowest level is (– α), and the base level is (0). Variable parameters can be coded using the following simple formula:

$$x_i = \frac{X_i - X_0}{\Delta X} \quad (3)$$

In this equation, x_i is the dimensionless coded value of the i th independent variable, X_i is the uncoded value of the i th test variable, X_0 is the real amount of independent variable in the central point, and ΔX is the step change value [24]. Central composite designs (CCD) are the most commonly used designs in the response surface methodology. This design, (CCD), consists of a full factorial or fractional design as well as a star design in which experimental points are at a distance α from its center and a center point. The total number of experiments is calculated using the following formula: $N = 2^k + 2k + c_p$, where k is the number of independent variable and c_p is the replicate number of the central point. The $2k$ denotes the number of star points with certain α [33]. The points in the full factorial

design are located at –1 and +1 levels; the points in star design are located at – α and + α levels, and the central point is located at level zero [31].

The new perspectives about neural networks emerged in the twentieth century when McCulloch and Pitts showed that neural networks could calculate every arithmetic and logical functions. Their work can be regarded as the starting point for the science of artificial neural networks (ANN), which is an effective modeling technique. Indeed, neural networks do not require the mathematical description of the phenomena involved in the process. Therefore, the simulation of the complicated systems is carried out more efficiently [34–36]. In the feed-forward networks, the neurons in each layer transmit the signals from the environment to the neurons in the next layers; in fact, the direction of the movement of signals is from input to output [34,37]; consequently, there is no feedback or loop. Standard back propagation is a gradient descent algorithm in which the network weights are moved along the negative of the gradient of the performance function [38]. A computational neural network consists of simple processing units called neuron [39]. Every network is composed of artificial neurons which have parallel connections with the other layers. The strength of these interconnections is determined by the weight associated with them [38,40]. For every ANN, the first layer constitutes the input layer (independent variables) and last one forms the output layer (dependent variables). One or more neuron layers called hidden layers can be located between them [37,39,41]. The number of neurons in the hidden layer can be determined by the desired accuracy in predictions. Therefore, it can be used as a parameter for designing neural networks [37,38,42].

One of disadvantages of ANN is the necessity for a large number of experimental data for training of network [36,43,44]. In the present study, a mathematical equation was obtained between the percentage of photocatalytic reduction of Cr(VI) and the operational parameters by RSM method. Using the obtained equation, some additional results were achieved, which were used for the first time in modeling the mentioned process using ANN. The accuracy of the model created by ANN was tested by the simulation of the experimental data used in RSM optimization.

2. Experimental setup

2.1. Materials

Potassium dichromate, nitric acid, and sodium hydroxide used in the study were purchased from

Merck (Germany). TiO₂-P25 was Degussa, constituting approximately 80% anatase and 20% rutile. It had a BET surface area of $50 \pm 15 \text{ m}^2 \text{ g}^{-1}$ and an average particle diameter of 21 nm, containing 99.5% TiO₂. The TEM image of the TiO₂-P25 nanoparticles is shown in Fig. 1. TEM image showed a wide heterogeneity in the size of the titania particles, ranging from ca. 10 to 50 nm.

2.2. The procedure

The nanoparticles of TiO₂-P25 in a slurry state were used in the study. First, a suspension of TiO₂-P25 nanoparticles in the desired pH was put under ultrasonic waves (Elma T460/H) in order to increase the dispersion of TiO₂ in water. Then, the obtained suspension was put inside a quartz tubular photoreactor equipped with a UV lamp (15 W, UV-C, manufactured by Philips, Holland) vertically placed in front of the reactor. A stream of oxygen was passed through the reactor at a flow rate of 0.8 mL min^{-1} and allowed to equilibrate for 15 min in the darkness. The photocatalytic reaction started when the UV lamp was switched on. Then, at defined intervals, 5 mL of the samples was taken and centrifuged (Hettich EBA). The concentration of Cr(VI) was measured by means of a UV-vis spectrophotometer (Ultrospec 2000, Biotech pharamcia, England) at 350 nm.

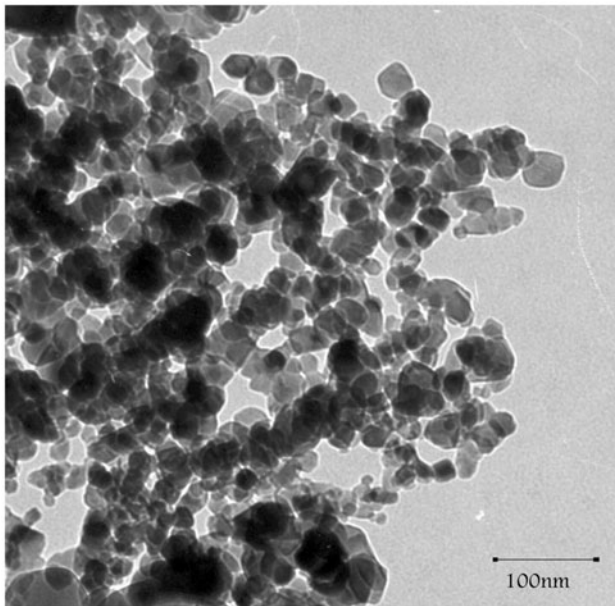


Fig. 1. TEM image of the TiO₂ nanoparticles.

The experimental data were analyzed by DX7 professional software for designing RSM. All ANN calculations were done using the mathematical software of Matlab 6.5 with an ANN toolbox. The three-layer network with sigmoid transfer function and a back propagation algorithm error were designed in this research. Sigmoid transfer function is the most widely used transfer function for the input and hidden layers. This function is nonlinear and is used in back propagation networks. This function receives the amount of input between $-\infty$ and $+\infty$ and produces an output between zero and one based on the following formula [43,45]:

$$a = \frac{1}{1 + e^{-n}} \quad (4)$$

To determine the optimum number of the hidden nodes, a series of topologies, in which a number of nodes change, were used. Mathematical functions such as mean square error (MSE) are usually used as error function, which can be obtained using the following equation [38,40]:

$$MSE = \frac{\sum_{i=1}^{i=N} (y_{i,\text{pred}} - y_{i,\text{exp}})^2}{N} \quad (5)$$

In which N is the number of data points, $y_{i,\text{pred}}$ is the network prediction, and $y_{i,\text{exp}}$ is the experimental response.

For sigmoid transfer function, all samples must fall within the range of 0.2–0.8. Therefore, all data groups (X_i) were turned into the new value of A_i as follows [41,46]:

$$A_i = 0.2 + \frac{0.6(X_i - \min(X_i))}{\max(X_i) - \min(X_i)} \quad (6)$$

Garson has proposed an equation based on partitioning of connection weights [47]:

$$I_j = \frac{\sum_{m=1}^{m=N_h} (|W_{jm}^{ih}| / \sum_{k=1}^{N_i} |W_{km}^{ih}|) \times |W_{mn}^{ho}|}{\sum_{k=1}^{k=N_i} \{ \sum_{m=1}^{m=N_h} (|W_{km}^{ih}| / \sum_{k=1}^{N_i} |W_{km}^{ih}|) \times |W_{mn}^{ho}| \}} \quad (7)$$

where I_j is the relative importance of the j th input variable on output variable, N_i and N_h are the number of input and hidden neurons, respectively, W 's are connection weights, the superscripts "i", "h", and "o" refer to input, hidden, and output layers, respectively, and subscripts "k", "m", and "n" refer to input, hidden, and output neurons, respectively.

3. Results and discussion

3.1. The optimization of the process of Cr(VI) photocatalytic reduction with RSM

3.1.1. Design of the experiment with RSM

To investigate the main and mutual effects of variables affecting the value of response in the process of Cr(VI) reduction TiO₂ nanoparticles, the RSM was utilized. The experiment was designed using CCD with reduced quadratic model. In this method, the effect of four independent factors of the initial concentration of Cr(VI), the dosage of TiO₂ catalyst, irradiation time, and pH on the value of the response was studied. The ranges and levels of these factors are given in Table 1. The experiments designed and the respective results are also shown in Table 2.

3.1.2. Response analysis

After obtaining the results of the experiments, the possibility of offering a suitable mathematical model between the independent variables (initial concentration of Cr(VI), the pH of the solution, the amount of TiO₂ nanocatalyst, and light irradiation time) and the value of the response (dependent variable) was investigated. The model in which the data were calculated mathematically was a reduced quadratic mathematical model. The coefficient of each of the parameters and other characteristics in the mathematical model are given in Table 3.

The obtained relation between the response (the percentage of reduction) and each of the factors is shown in the following equation:

$$R = 36.63 - 7.80 \times A - 11.72 \times B + 5.69 \times C + 4.00 \times D - 0.14 \times AB + 0.42 \times BD + 0.43 \times A^2 - 1.00 \times B^2 \quad (8)$$

where R is the efficiency or the percentage of Cr(VI) reduction (response). A , B , C , and D are parameters and coefficients obtained through linear effects regression,

the mutual effects of coefficients (AB and BD) are obtained through interaction effects regression of parameters, and the coefficients of A^2 and B^2 are obtained through quadratic effects regression.

According to this equation, the parameters which had significant effects were the initial concentration of Cr(VI) (A), pH of solution (B), the amount of TiO₂ nanocatalyst (C), the light radiation time (D), the mutual effects of the two parameters of initial concentration of the pollutant and pH of the solution (AB), the mutual effects of the two parameters of solution pH and the irradiation time (BD), the square root of the initial concentration of Cr(VI) (A^2), and the square root of solution pH (B^2).

To analyze the responses and variables, the analysis of variance was used. The results are given in Table 4.

The value of R^2 is an index for measuring the range of variability in the observed response. The results indicate that this model has a correlation coefficient of $R^2 = 0.9812$. The value of R^2 reveals that 98.12% of the changes occurred in the efficiency of reduction by independent variables. The model failed to account for only 1.88% of the changes.

To examine the validity of the model, the residual values (difference between the experimental and predicted response values) were calculated. Fig. 2 shows the dispersion of the residual values. The linear nature of the normal probability plot for the residuals indicates that the proposed model is correct.

Fig. 3 shows the residual values vs. the number of experiments. The random distribution of the residual values about zero indicates the accuracy of the selected model.

3.1.3. RSM design and three dimensional graphs

In order to observe and study the effect of the parameters on the response, respective three-dimensional figures were drawn. Since it is not possible to draw more than three dimensions on the screen, the effect of the parameters on response was reported

Table 1
Factors and their levels in designing experiments with RSM method

Factor	Range and levels				
	$-\alpha$	-1	0	+1	$+\alpha$
Initial concentration of Cr(VI) (mg L ⁻¹)	15	20	25	30	35
pH of the solution	1	2	3	4	5
Dosage of TiO ₂ nanocatalyst (mg L ⁻¹)	100	150	200	250	300
Irradiation time (min)	7.5	15	22.5	30	37.5

Table 2

The experiments designed with RSM and the respective experimental results

Number of experiments	Factors and the obtained experimental responses				Experimental responses % R_{EXP}
	A: [Cr] (mg L ⁻¹)	B: pH	C: TiO ₂ (mg L ⁻¹)	D: Time (min)	
1	20	2	150	15	43.3
2	30	2	150	15	31.37
3	20	4	150	15	25.66
4	30	4	150	15	5.88
5	20	2	250	15	59.64
6	30	2	250	15	40.85
7	20	4	250	15	28.92
8	30	4	250	15	20.15
9	20	2	150	30	55.07
10	30	2	150	30	38.56
11	20	4	150	30	31.7
12	30	4	150	30	15.36
13	20	2	250	30	61.8
14	30	2	250	30	49.35
15	20	4	250	30	43.46
16	30	4	250	30	26.47
17	15	3	200	22.50	54.68
18	35	3	200	22.50	21.84
19	25	1	200	22.50	57.25
20	25	5	200	22.50	7.84
21	25	3	100	22.50	22.74
22	25	3	300	22.50	49.15
23	25	3	200	7.50	27.71
24	25	3	200	37.50	42.74
25	25	3	200	22.50	37.91
26	25	3	200	22.50	34.12
27	25	3	200	22.50	35.03
28	25	3	200	22.50	37.91
29	25	3	200	22.50	40.52
30	25	3	200	22.50	38.17

Table 3

The coefficient of each parameter in the reduced quadratic mathematic model

Factor	Coefficient estimate	Degree of freedom	Standard error
Intercept	36.63	1	0.67
A: ([Cr] ₀)	-7.8	1	0.48
B: pH	-11.72	1	0.48
C: TiO ₂	5.69	1	0.48
D: Time	4	1	0.48
AB	-0.14	1	0.58
BD	0.42	1	0.58
A ²	0.43	1	0.44
B ²	-1	1	0.44

Table 4
ANOVA results for the response surface reduced quadratic model for reduction Cr(VI)

Source	Sum of squares	Degree of freedom	Mean square	F-value	p-Value prob > F	Situation
Model	5956.13	8	744.52	136.64	<0.0001	Significant
LOF	87.29	16	5.46	1.01	0.5482	Not significant
$R^2 = 0.9812$						
$R^2_{adj} = 0.9740$						

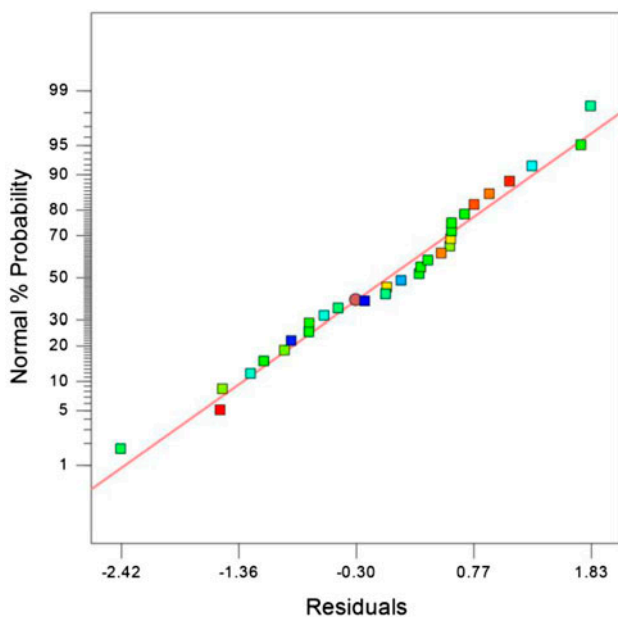


Fig. 2. Normal probability plot of residuals for photocatalytic reduction efficiency of Cr(VI).

in pairs. Fig. 4 shows the effect of the initial concentration of Cr(VI) and the pH of the solution on the efficiency of Cr(VI) reduction. The figure indicates the fact that with the increase in the initial concentration of Cr(VI), the percentage of reduction decreases. The reason is the fact that the absorption of solution goes up with the increase in $K_2Cr_2O_7$ concentration. As a result, the greater amount of the radiated UV is absorbed by Cr solution before reaching the photocatalyst surface causing lower percentage of Cr(VI) photoreduction [5,48]. The graph demonstrates that maximum amount of efficiency for photocatalytic reduction is observed at pH 2. The catalyst surface gets positive charge as a result of proton absorption, and $Cr_2O_7^{2-}$, which carries negative charge that could better approach it and the reduction is facilitated by the excited electrons [22,23].

Fig. 5 also shows the effect of pH and the light irradiation time on the efficiency of Cr(VI) reduction by TiO_2 nanoparticles. The figure indicates that the

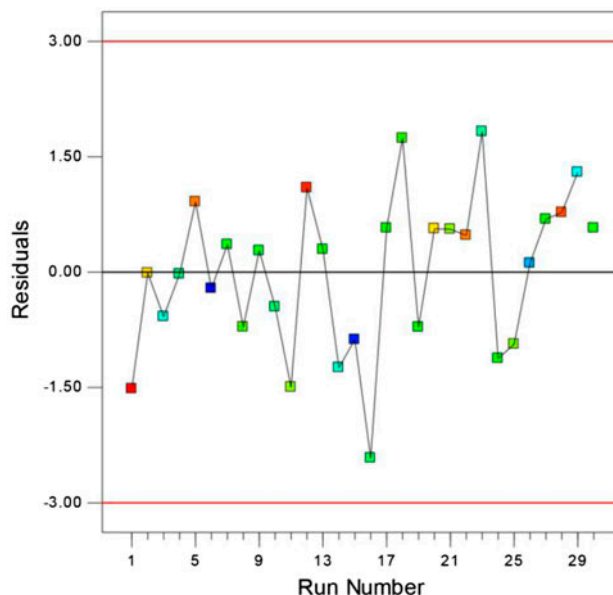


Fig. 3. The residual values vs. run number for photocatalytic reduction efficiency of Cr(VI).

photocatalytic Cr(VI) reduction increases with the enhancement of irradiation time. Because with increased irradiation time, more electrons are excited, causing the percentage of Cr(VI) reduction to increase [6,49]. The maximum efficiency of Cr(VI) reduction by TiO_2 nanoparticles in the RSM design is approximately 60%. Fairly low efficiency of Cr(VI) reduction to Cr(III) can be related to the deactivation of the catalyst due to Cr(III) deposition on the catalyst surface [50].

A comparison between experimental results and the results predicted through RSM are shown in Fig. 6. The value of $R^2 = 0.9812$ indicates the correspondence between the experimental data and the data predicted by RSM.

3.2. ANN modeling of photocatalytic of Cr(VI) reduction

The topology of an ANN is determined by the number of layers, the number of nodes in each layer, and the nature of transfer functions [40]. For ANN modeling of Cr(VI) photocatalytic reduction with TiO_2

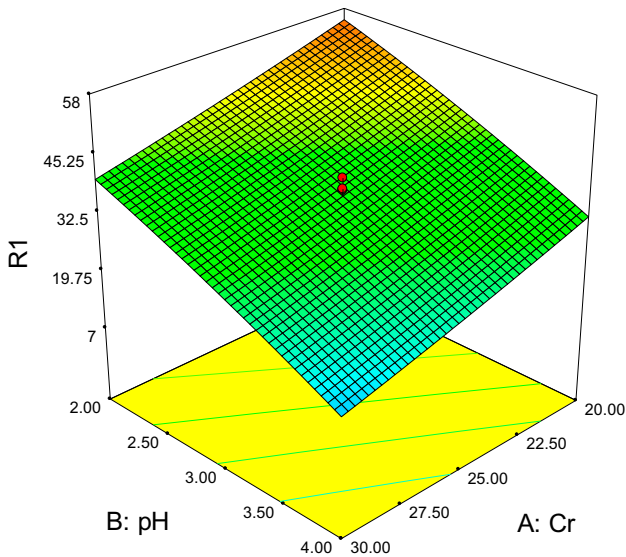


Fig. 4. Three dimensional graph of the effect of initial concentration of Cr(VI) and pH on the efficiency of Cr(VI) photocatalytic reduction by TiO₂ nanoparticles.

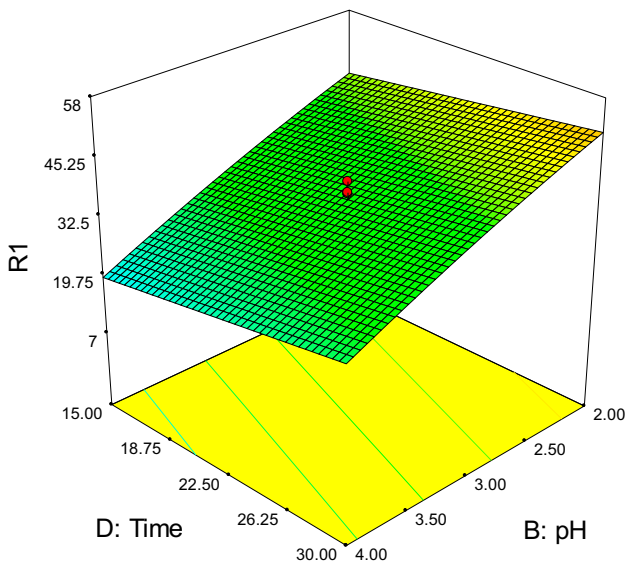


Fig. 5. Three-dimensional graph of the effect of pH and light irradiation time on the efficiency of Cr(VI) photocatalytic reduction by TiO₂ nanoparticles.

nanoparticles, a three-layer feed-forward back propagation was used. This network consisted of four neurons in the input layer, four neurons in hidden layer, and one neuron in output layer (Fig. 7).

As shown in Fig. 7, the input variables include the initial concentration of Cr(VI), the amount of TiO₂ catalyst, light irradiation time, and pH. The number of neurons in the hidden layer defines the topology of a

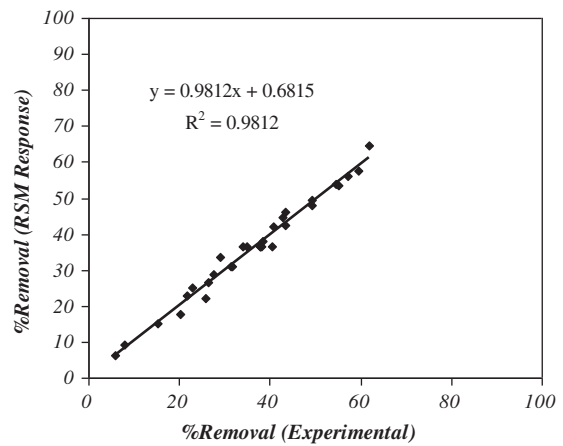


Fig. 6. Comparison between experimental results and predicted values from RSM.

feed-forward network. To determine the optimum number of neurons in the hidden layer, different topologies of 1–5 neurons were conducted. The MSE was used in every topology as the error function. Fig. 8 shows MSE vs. the number of neurons in the hidden layer.

As this figure shows, the minimum MSE can be obtained with the inclusion of four neurons in the hidden layer. In this study, a sigmoid transfer function was used in the hidden layer, and a pureline function was used in the output layer as transfer function.

One of the problems in ANN modeling is the need for a large quantity of experimental data. In the present study, for the first time, the results of RSM-based mathematical equation were used for training ANN. Since the study examined four parameters at five levels examined here, for RSM, there could be a total of 625 pieces of data for ANN modeling, out of which

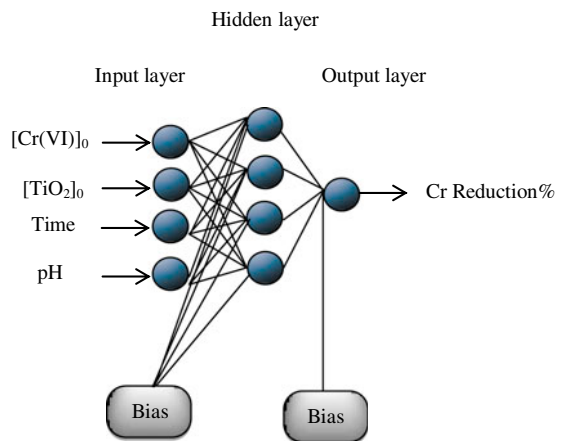


Fig. 7. The optimal structure of ANN.

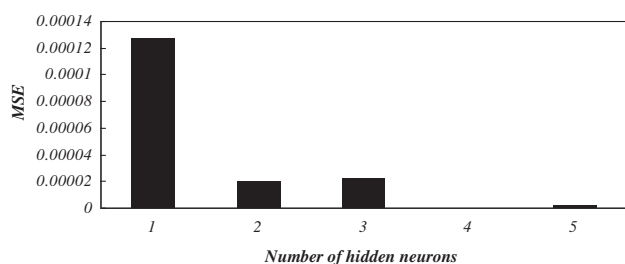


Fig. 8. Effect of the number of neurons in the hidden layer on the performance of the neural network.

558 data were selected and used for training, validating, and testing the network. Moreover, to simulate the network, 25 data used for RSM design were utilized. From 558 data, 60% were randomly selected for training, 20% for validation, and 20% for testing. Based on sigmoid transfer function, all data must be scaled between 0.2 and 0.8 range. To calculate training validation and test errors, all the data were re-converted into the original scale to be compared with the original responses.

3.2.1. Testing of the ANN model

To test the precision of the ANN model a comparison was made between the modeling and experimental results. Fig. 9(a) shows the comparison between RSM-based data and the data obtained from ANN model with four neurons in the hidden layer.

The results in Fig. 9(a) indicate that ANN is able to get appropriate training from RSM-based data due to the high amount of input data, since the amount of R^2 and the slope of the obtained line is 1 and the intercept of the obtained line is very near to zero. To ensure appropriate network training, 25 experimental data, which had not been used in ANN, were used for simulation. The comparison between the ANN-based results and those of RSM for 25 data as well as for the experimental results is shown in Fig. 9(b) and (c), respectively. The results confirm that the neural network model trained with data obtained from RSM-based mathematical equation is able to sufficiently predict the photocatalytic reduction of Cr(VI). Having ensured the appropriateness of ANN training, network weight matrices were obtained and reported in Table 5, in which W_1 is the weight between the input

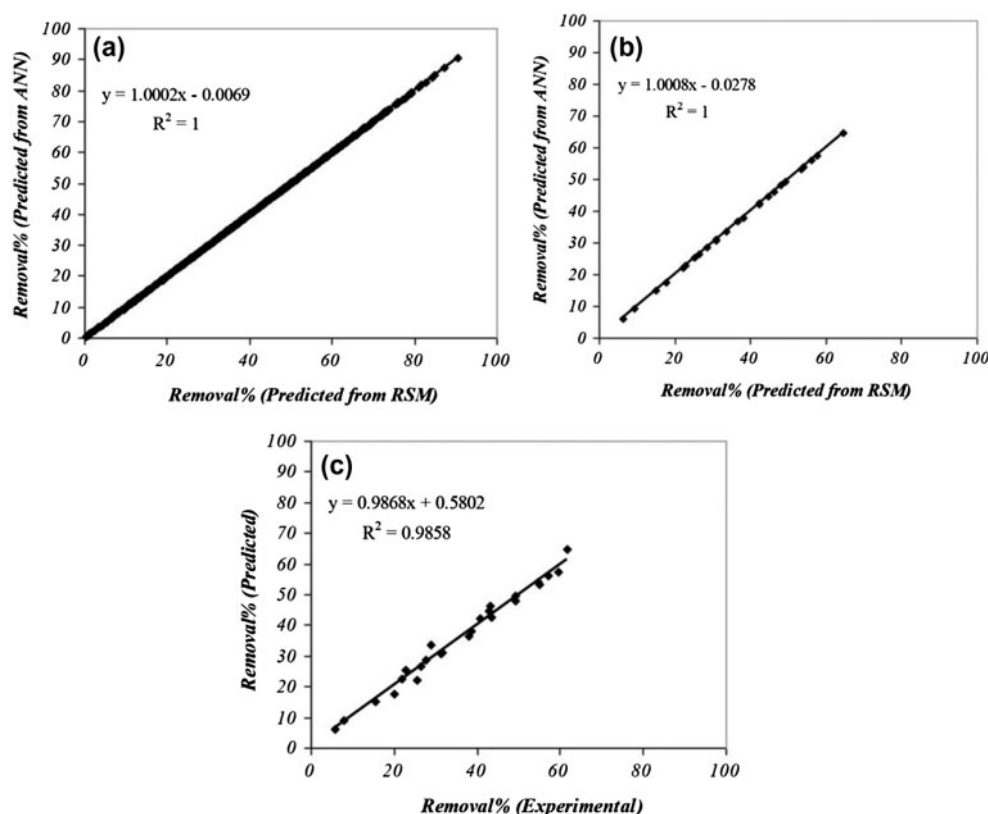


Fig. 9. Comparison between the data from RSM-based mathematical equation and the data from ANN for all data (a), Simulation of the RSM data with ANN (b), Simulation of the experimental data with ANN (c).

Table 5
Matrices of weights

W ₁					W ₂		
Neuron	Variable				Bias	Neuron	Weight
–	[Cr(VI)] ₀	pH	[TiO ₂] ₀	Time			
1	1.5395	–0.4008	–0.1169	–6.9449	–5.2240	1	0.0084
2	0.0969	0.0287	–0.1399	–0.0434	0.0127	2	–7.2532
3	–0.0413	–0.6758	–0.0004	0.1434	1.3402	3	4.2365
4	0.9760	–0.0182	0.0007	–0.0173	1.3787	4	–0.9108
						Bias	0.8237

Table 6
Relative importance of the input variables in the percentage of Cr(VI) reduction

Input variable	Importance (%)
Initial concentration of Cr(VI)	27.07
Initial amount of TiO ₂ nanocatalyst	26.49
Irradiation time	14.07
Initial pH	32.37

and hidden layers, and W_2 is the weight between the hidden and output layers. Weights are the coefficients between the artificial neurons which act like synapse strengths between the axons and dendrites in real biologic neurons. Therefore, each weight determines what proportion of the input signal will be transferred to the body of the neuron.

Using the matrices of the weights in Table 5 and Eq. (7), the importance of the input variables in the percentage of Cr(VI) reduction was calculated. All the input variables affected the percentage of Cr(VI) reduction, but the effect of pH was more than the others. This is shown in Table 6.

4. Conclusions

The results indicate that the data obtained from RSM-based mathematical equation could be used to model artificial neural network. The number of neurons in the hidden layer is among the parameters affecting artificial neural network model. Therefore, by changing the number of neurons in the hidden layer, the least value of errors is observed with four neurons. The study showed that the results from ANN corresponded with those from RSM and the experimental data. Therefore, it may be concluded that RSM can be used for the production of data-sets needed for ANN modeling.

Acknowledgments

Thanks to the Tabriz Branch, Islamic Azad University and the Iranian Nanotechnology Initiative Council for their financial support.

References

- [1] S.H. Lin, C.N. Chen, R.S. Juang, Structure and thermal stability of toxic chromium (VI) species doped onto TiO₂ powders through heat treatment, *J. Environ. Manage.* 90 (2009) 1950–1955.
- [2] G. Colón, M.C. Hidalgo, J.A. Navío, Photocatalytic deactivation of commercial TiO₂ samples during simultaneous photoreduction of Cr(VI) and photooxidation of salicylic acid, *J. Photochem. Photobiol., A* 138 (2001) 79–85.
- [3] B. Galán, D. Castañeda, I. Ortiz, Removal and recovery of Cr(VI) from polluted ground waters: A comparative study of ion-exchange technologies, *Water Res.* 39 (2005) 4317–4324.
- [4] N. Wang, L. Zhu, K. Deng, Y. She, Y. Yu, H. Tang, Visible light photocatalytic of Cr(VI) on TiO₂ *in situ* modified with small molecular weight organic acids, *Appl. Catal., B* 95 (2010) 400–407.
- [5] S. Chakrabarti, B. Chaudhuri, S. Bhattacharjee, A.K. Ray, B.K. Dutta, Photo-reduction of hexavalent chromium in aqueous solution in the presence of zinc oxide as semiconductor catalyst, *Chem. Eng. J.* 153 (2009) 86–93.
- [6] X. Domenech, J. Munoz, Photochemical elimination of Cr(VI) from neutral-alkaline solutions, *J. Chem. Technol. Biotechnol.* 47 (1990) 101–107.
- [7] Z. Yue, S.E. Bender, J. Wang, J. Economy, Removal of chromium Cr(VI) by low-cost chemically activated carbon materials from water, *J. Hazard. Mater.* 166 (2009) 74–78.
- [8] Q. Wang, J. Shang, T. Zhu, F. Zhao, Efficient photoelectrocatalytic reduction of Cr(VI) using TiO₂ nanotube arrays as the photoanode and a large-area titanium mesh as the photocathode, *J. Mol. Catal. A: Chem.* 335 (2011) 242–247.
- [9] F.Di. Natale, A. Lancia, A. Molino, D. Musmarra, Removal of chromium ions from aqueous solutions by adsorption on activated carbon and char, *J. Hazard. Mater.* 145 (2007) 381–390.

- [10] P. Mohapatra, S.K. Samantaray, K. Parida, Photocatalytic reduction of hexavalent chromium in aqueous solution over sulphate modified titania, *J. Photochem. Photobiol., A* 170 (2005) 189–194.
- [11] S.L. Wang, C.C. Chen, Y.M. Tzou, C.L. Hsu, J.H. Chen, C.F. Lin, A mechanism study of light-induced Cr(VI) reduction in an acidic solution, *J. Hazard. Mater.* 164 (2009) 223–228.
- [12] P. Mytych, Z. Stasicka, Photochemical reduction of chromium(VI) by phenol and its halogen derivatives, *Appl. Catal., B* 52 (2004) 167–172.
- [13] L. Wang, N. Wang, L. Zhu, H. Yu, H. Tang, Photocatalytic reduction of Cr(VI) over different TiO₂ photocatalysts and the effects of dissolved organic species, *J. Hazard. Mater.* 152 (2008) 93–99.
- [14] S. Rengaraj, S. Venkataraj, J.W. Yeon, Y. Kim, X.Z. Li, G.K.H. Pang, Preparation, characterization and application of Nd-TiO₂ photocatalyst for the reduction of Cr(VI) under UV light illumination, *Appl. Catal., B* 77 (2007) 157–165.
- [15] S. Gupta, B.V. Babu, Removal of toxic metal Cr(VI) from aqueous solutions using sawdust as adsorbent: Equilibrium, kinetics and regeneration studies, *Chem. Eng. J.* 150 (2009) 352–365.
- [16] K. Tarangini, A. Kumar, G.R. Satpathy, V.K. Sangal, Statistical optimization of process parameters for Cr(VI) biosorption onto mixed cultures of *Pseudomonas aeruginosa* and *Bacillus subtilis*, *Clean: Soil Air Water* 37 (2009) 319–327.
- [17] V. Gupta, A. Rastogi, A. Nayak, Adsorption studies on the removal of hexavalent chromium from aqueous solution using a low cost fertilizer industry waste material, *J. Colloid Interface Sci.* 342 (2010) 135–141.
- [18] S. Gupta, B.V. Babu, Modeling, simulation, and experimental validation for continuous Cr(VI) removal from aqueous solutions using sawdust as an adsorbent, *Bioresour. Technol.* 100 (2009) 5633–5640.
- [19] J. Yoon, E. Shim, S. Bae, H. Joo, Application of immobilized nanotubular TiO₂ electrode for photocatalytic hydrogen evolution: Reduction of hexavalent chromium (Cr(VI)) in water, *J. Hazard. Mater.* 161 (2009) 1069–1074.
- [20] A.K. Golder, A.K. Chanda, A.N. Samanta, S. Ray, Removal of hexavalent chromium by electrochemical reduction-precipitation: Investigation of process performance and reaction stoichiometry, *Sep. Purif. Technol.* 76 (2011) 345–350.
- [21] M. Kebir, M. Chabani, N. Nasrallah, A. Bensmaili, M. Trari, Coupling adsorption with photocatalysis process for the Cr(VI) removal, *Desalination* 270 (2011) 166–173.
- [22] J.A. Navío, G. Colón, M. Trillas, J. Peral, X. Domènech, J.J. Testa, J. Padrón, D. Rodríguez, M.I. Litter, Heterogeneous photocatalytic reactions of nitrite oxidation and Cr(VI) reduction on iron-doped titania prepared by the wet impregnation method, *Appl. Catal. B* 16 (1998) 187–196.
- [23] S. Wang, Z. Wang, Q. Zhuang, Photocatalytic reduction of the environmental pollutant Cr^{VI} over a cadmium sulphide powder under visible light illumination, *Appl. Catal., B* 1 (1992) 257–270.
- [24] K.S. Rao, S. Anand, K. Rout, P. Venkateswarlu, Response surface optimization for removal of cadmium from aqueous solution by waste agricultural biosorbent *Psidium guajava* L. leaf powder, *Clean: Soil Air Water* 40 (2012) 80–86.
- [25] M. Fathinia, A.R. Khataee, M. Zarei, S. Aber, Comparative photocatalytic degradation of two dyes on immobilized TiO₂ nanoparticles: Effect of dye molecular structure and response surface approach, *J. Mol. Catal. A: Chem.* 333 (2010) 73–84.
- [26] A.R. Khataee, G. Dehghan, E. Ebadi, M. Pourhassan, Central composite design optimization of biological dye removal in the presence of macroalgae *chara* sp., *Clean: Soil Air Water* 38 (2010) 750–757.
- [27] A.R. Khataee, Application of central composite design for the optimization of photo-destruction of a textile dye using UV/S₂O₈²⁻ process, *Pol. J. Chem. Technol* 4 (2009) 38–45.
- [28] A.R. Khataee, Optimization of UV-promoted peroxydisulphate oxidation of C.I. Basic Blue 3 using response surface methodology, *Environ. Technol.* 31 (2010) 73–86.
- [29] K. Anupam, S. Dutta, C. Bhattacharjee, S. Datta, Adsorptive removal of chromium (VI) from aqueous solution over powdered activated carbon: Optimisation through response surface methodology, *Chem. Eng. J.* 173 (2011) 135–143.
- [30] C. Betianu, F.A. Caliman, M. Gavrilescu, I. Cretescu, C. Cojocar, I. Poullos, Response surface methodology applied for orange II photocatalytic degradation in TiO₂ aqueous suspensions, *J. Chem. Technol. Biotechnol.* 83 (2008) 1454–1465.
- [31] J. Zolgharnein, N. Asanjarani, S.N. Mousavi, Optimization and characterization of Tl(I) adsorption onto Modified *Ulmus carpinifolia* tree leaves, *Clean: Soil Air Water* 39 (2010) 250–258.
- [32] Z. Khalili, B. Bonakdarpour, Statistical optimization of anaerobic biological processes for dye treatment, *Clean: Soil Air Water* 38 (2010) 942–950.
- [33] V.A. Sakkas, Md. A. Islam, C. Stalikas, T.A. Albanis, Photocatalytic degradation using design of experiments: A review and example of the Congo red degradation, *J. Hazard. Mater.* 175 (2010) 33–44.
- [34] S. Göb, E. Oliveros, S.H. Bossmann, A.M. Braun, C.A.O. Nascimento, R. Guardani, Optimal experimental design and artificial neural networks applied to the photochemically enhanced Fenton reaction, *Water Sci. Technol.* 44 (2001) 339–345.
- [35] A.R. Khataee, A. Khani, Modeling of nitrate adsorption on granular activated carbon (GAC) using artificial neural network (ANN), *Int. J. Chem. Reactor Eng.* 7 (2009). Available from: <http://www.degruyter.com/view/j/ijcre.2009.7.1/ijcre.2009.7.1.1870/ijcre.2009.7.1.1870.xml>.
- [36] N. Daneshvar, A.R. Khataee, N. Djafarzadeh, The use of artificial neural networks (ANN) for modeling of decolorization of textile dye solution containing C. I. Basic Yellow 28 by electrocoagulation process, *J. Hazard. Mater.* 137 (2006) 1788–1795.
- [37] A.R. Khataee, M.B. Kasiri, Modeling of biological water and wastewater treatment processes using artificial neural networks, *Clean: Soil Air Water* 39 (2011) 742–749.
- [38] A.R. Khataee, M.B. Kasiri, Artificial neural networks modeling of contaminated water treatment processes by homogeneous and heterogeneous nanocatalysis, *J. Mol. Catal. A: Chem.* 331 (2010) 86–100.

- [39] A. Aleboyeh, M.B. Kasiri, M.E. Olya, H. Aleboyeh, Prediction of azo dye decolorization by UV/H₂O₂ using artificial neural networks, *Dyes Pigm.* 77 (2008) 288–294.
- [40] A.R. Khataee, M. Zarei, M. Pourhassan, Application of microalga *Chlamydomonas* sp. for biosorptive removal of a textile dye from contaminated water: Modelling by a neural network, *Environ. Technol.* 30 (2009) 1615–1623.
- [41] D. Salari, N. Daneshvar, F. Aghazadeh, A.R. Khataee, Application of artificial neural networks for modeling of the treatment of wastewater contaminated with methyltert-butyl ether (MTBE) by UV/H₂O₂ process, *J. Hazard. Mater.* 125 (2005) 205–210.
- [42] S. Dutta, S.A. Parsons, C. Bhattacharjee, S. Bandhyopadhyay, S. Datta, Development of an artificial neural network model for adsorption and photocatalysis of reactive dye on TiO₂ surface, *Expert Syst. Appl.* 37 (2010) 8634–8638.
- [43] A.R. Khataee, Photocatalytic removal of C.I. Basic Red 46 on immobilized TiO₂ nanoparticles: Artificial neural network modeling, *Environ. Technol.* 30 (2009) 1155–1168.
- [44] F. Ghanbary, N. Modirshahla, M. Khosravi, M.A. Behnajady, Synthesis of TiO₂ nanoparticles in different thermal conditions and modeling its photocatalytic activity with artificial neural network, *J. Environ. Sci.* 24 (2012) 750–756.
- [45] A. Niaei, J. Towfighi, A.R. Khataee, K. Rostamizadeh, The use of ANN and mathematical model for prediction of the main product yields in the thermal cracking of naphtha, *Pet. Sci. Technol.* 25 (2007) 967–982.
- [46] M. Zarei, A.R. Khataee, R. Ordikhani-Seyedlar, M. Fathinia, Photoelectro-Fenton combined with photocatalytic process for degradation of an azo dye using supported TiO₂ nanoparticles and carbon nanotube cathode: Neural network modeling, *Electrochim. Acta.* 55 (2010) 7259–7265.
- [47] G.D. Garson, Interpreting neural-network connection weights, *AI Expert.* 6 (1991) 47–51.
- [48] K. Kabra, R. Chaudhary, R.L. Sawhney, Treatment of hazardous organic and inorganic compounds through aqueous-phase photocatalysis: A review, *Ind. Eng. Chem. Res.* 43 (2004) 7683–7696.
- [49] L.B. Khalil, W.E. Mourad, M.W. Rophael, Photocatalytic reduction of environmental pollutant Cr(VI) over some semiconductors under UV/visible light illumination, *Appl. Catal., B* 17 (1998) 267–273.
- [50] J. Sabate, M.A. Anderson, Comparison of TiO₂ powder suspensions and TiO₂ ceramic membranes supported on glass as photocatalytic systems in the reduction of chromium(VI), *J. Mol. Catal.* 71 (1992) 57–68.